Improved Fisher MAP Filter for Despeckling of High-Resolution SAR Images Based on Structural Information Detection

Wei Wei[1, 2], Zeng-Guo Sun[3], Zhi-Hua Zhang[4], Rafal Scherer[5], Robertas Damaševičius[6]
[1] College of Computer Science and Engineering, Xi'an University of Technology, China
[2] Shaanxi Key Laboratory for Network Computing and Security Technology, China
[3] School of Computer Science, Shaanxi Normal University, China
[4] College of Computer Science and Technology, Huaqiao University, China
[5] Czestochowa University of Technology, Poland
[6] Department of Applied Informatics, Vytautas Magnus University, Lithuania
weiwei@xaut.edu.cn, sunzg@snnu.edu.cn, 18030126723@163.com, rafal.scherer@pcz.pl, robertas.damasevicius@vdu.lt

Abstract

Fisher distribution is a popular model for high-resolution (HR) synthetic aperture radar (SAR) images due to its high-peaked and heavy-tailed characteristics as well as its theoretical justification and mathematical tractability. Based on the Fisher modeling of SAR images, the maximum a posteriori (MAP) filter is suggested. In the Fisher model, the parameter of image looks is thought to be fixed to correspond to the formation mechanism of multi-look intensity images, and the other two parameters are accur ately assessed from the SAR image based on second-kind statistics. To improve the Fisher MAP filter especially in the aspect of speckle suppression, the Fisher MAP filter based on recognition of structural information is created using point target detection, the adaptive windowing method, homogeneous region detection, and selection of most homogeneous sub-window. The experiments on despeckling of HR SAR images demonstrate that the improved Fisher MAP filter based on structural information detection can suppress speckle in homogenous and edge regions, and effectively preserve fine details, edges, and point targets.

Keywords: Fisher filter, High-resolution synthetic aperture radar image, Structural information detection, Second-kind statistics

1 Introduction

Synthetic aperture radar (SAR) images are corrupted by speckle, which reduces quality of images and makes the post-processing of images extremely difficult [1]. Therefore, despeckling algorithms are indispensable to accurate understanding of SAR images. For a promising despeckling algorithm, an appropriate distribution of SAR image should be taken into consideration [2-5]. The traditional Rayleigh distribution works well for low-resolution SAR images [6], but it does not perform well on high-resolution (HR) SAR images [6-10]. The log-normal and Weibull distributions are better choices for modeling specific SAR images [11], but they are empirical models, which lack theoretical justification [12-14]. Recently, Fisher distribution, has drawn considerable attention for modeling HR-SAR images, specifically for urban regions, due to its high peak and heavy tail statistical characteristics [15-17]. The Fisher model is strictly derived from the multiplicative model of speckle and the Mellin convolution, owning more theoretical justification and mathematical tractability compared with the log-normal and Weibull [18-19].

In this paper, using Fisher model, the maximum a posteriori (MAP) filter is proposed for high-resolution SAR images. It must be stressed that the parameter of image looks in the Fisher model is fixed, which corresponds to the practical formation mechanism of multi-look intensity images [1]. Under this condition, the Fisher MAP filter only depends on the estimated values of the other two parameters of Fisher model. Recently, a powerful tool called second-kind statistics that relies on the Mellin transformation has been generally exploited to accurately estimate the parameters of some sophisticated distributions for SAR images [18-22]. Motivated by the second-kind statistics, the log-cumulant estimators are presented to accurately estimate the other two parameters of Fisher model from the observed image, and then the Fisher MAP filter can be readily performed. To improve the Fisher MAP filter especially in the aspect of speckle suppression, the Fisher MAP filter based on detection of structural information is constructed. The process includes detection of point target, application of adaptive windowing, detection of the homogeneous region, and selection of the most homogeneous sub-

*Corresponding Author: Zeng-Guo Sun; E-mail: sunzg@snnu.edu.cn
DOI: 10.3966/160792642021032202016

window [23-25]. We demonstrate the performance of the improved Fisher MAP filter, for despeckling of HR-SAR images. The results show a good trade-off between elimination of speckle and preservation of edges, fine details, and point targets.

2 Fisher Distribution

The probability density function (pdf) of Fisher distribution is defined as:

$$f(x)=\frac{\Gamma(L+M)}{\Gamma(L)\Gamma(M)}\left(\frac{Lx}{M\mu}\right)^{L-1}\left(1+\frac{Lx}{M\mu}\right)^{-(L+M)} \qquad \textbf{(1)}$$

where L is the image looks, M ($M>0$) is the shape parameter, μ ($\mu>0$) is the scale parameter, and $\Gamma(\cdot)$ denotes the Gamma function.

To show the merit of the Fisher distribution in modeling HR-SAR images, a HR-SAR image shown in Figure 1 was modeled by the Fisher distribution as well as other distributions such as Rayleigh, log-normal, and Weibull.

Figure 1. X-Band HR-SAR image (1-m resolution)

The modeling results are presented in Figure 2. The use of logarithmic scale is to detail the fitting degree of various distributions to the tail of image.

Obviously, the HR-SAR image owns the high-peak and heavy-tail characteristics, and only the Fisher distribution can accurately describe such characteristics of high peak and heavy tail simultaneously. Therefore, it is reasonable to believe that the MAP filter that uses Fisher modeling of SAR images performs well especially in preservation of edges and fine details [26-28].

3 Fisher MAP Filter

The general form of the MAP equation is given by

$$-\frac{1}{X}+\frac{\partial \ln f_F(F)}{\partial X}+\frac{\partial \ln f_F(X)}{\partial X}\Big|_{X=\hat{X}_{MAP}}=0 \qquad \textbf{(2)}$$

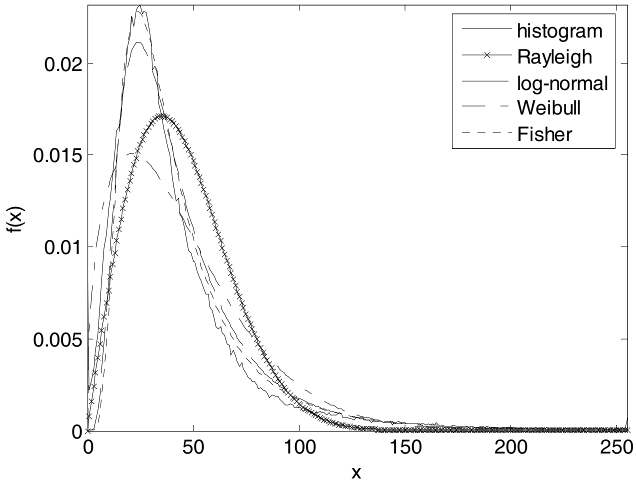

(a) Linear scale

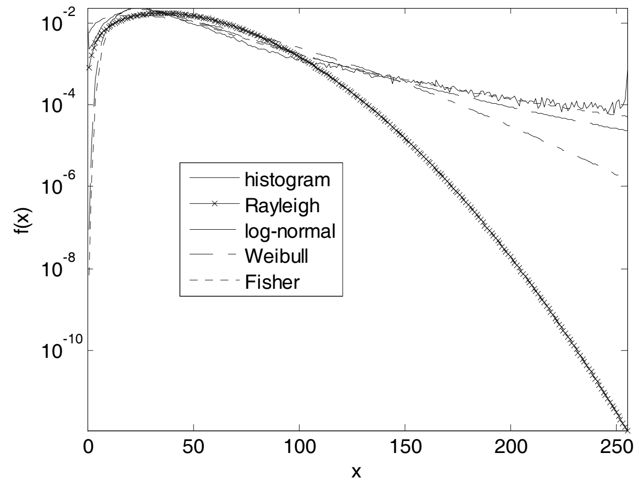

(b) Logarithmic scale

Figure 2. Modeling the SAR image in Figure 1 using various distributions

here F is the speckle, X is the true image not corrupted by speckle, f_F and f_X are the pdfs of F and X respectively, and $\hat{X}_{MAP}$ is the MAP estimate of X [29-31].

Obviously, distributions of the speckle and the ground truth image are needed for the MAP formula. In the derivation of Fisher distribution, the Gamma and inverse Gamma distributions are used to describe the speckle and the true image respectively, and then the Fisher MAP equation is constructed according to (2).

For a L -look intensity image, speckle statistically obeys the Gamma probability distribution, with the following PDF:

$$f_F(x)=\frac{L^L x^{L-1} e^{-Lx}}{\Gamma(L)} \qquad \textbf{(3)}$$

where L is the image looks [19]. On the other hand, the true image is modeled by the inverse Gamma distribution, whose pdf is given by

$$f_X(x) = \frac{1}{\Gamma(M)}(\frac{M}{\mu})^M x^{-(M+1)} e^{-\frac{M}{\mu x}}, \quad \textbf{(4)}$$

where $M\,(M>0)$ is the shape parameter, and $\mu\,(\mu>0)$ is the scale parameter [32]. Substituting (3) and (4) into (2), the Fisher MAP equation is obtained by

$$(1+L+M)\mu\hat{X} - \mu LY - M = 0, \quad \textbf{(5)}$$

where $\hat{X}$ is the MAP estimate of *X* and *Y* denotes the observed image.

Finally, the output of the Fisher MAP filter is straightforward

$$\hat{X} = \frac{LY + \frac{M}{\mu}}{1+L+M}. \quad \textbf{(6)}$$

Three parameters *L*, *M* and μ appear in (6). The parameter *L*, which appears in the pdf of Gamma distribution for speckle, is closely relevant to the formation mechanism of multi-look intensity images [1]. For a single-look intensity image, speckle is statistically modeled by the exponential distribution. After averaging *L* single-look intensity images, a *L* -look intensity image is formed, and the speckle in the *L* -look intensity image is statistically described by the Gamma probability distribution with *L* looks in (3). In fact, the *L* -look Gamma distribution is strictly derived from *L* convolutions of exponential distribution. Therefore, for a specific *L* -look intensity image, the value of *L* is fixed and not needed to be estimated [19, 32].

For the use of the Fisher MAP filter, the only parameters *M* and μ are required to be estimated, which reduces computational load and improves running efficiency of the Fisher MAP filter.

4 Log-cumulant Parameter Estimators Based On Second-kind Statistics

The second-kind statistics are constructed theoretically based on the Mellin transformation [33-34]. Denoting *f* as a pdf defined in $[0,\infty)$, the second-kind statistics are defined successively as follows, including the second-kind first characteristic function $\Phi(s)$ and the second characteristic function $\psi(s)$, and the *r* -th order log-cumulant $\tilde{k}_r$ [31]:

$$\Phi(s) = \int_0^\infty x^{s-1} f(x)dx, \quad \textbf{(7)}$$

$$\psi(s) = \ln\Phi(s), \quad \textbf{(8)}$$

$$\tilde{k}_r = \frac{d^r\psi(s)}{ds^r}|_{s=1}. \quad \textbf{(9)}$$

The log-cumulants $\tilde{k}_1$ and $\tilde{k}_2$ can be computed from the observed samples y_i as

$$\hat{\tilde{k}}_1 = \frac{1}{N}\sum_{i=1}^{N}\ln y_i, \hat{\tilde{k}}_2 = \frac{1}{N-1}\sum_{i=1}^{N}(\ln y_i - \hat{\tilde{k}}_1)^2. \quad \textbf{(10)}$$

Here, *N* is the number of samples.

The widely used multiplicative model of speckle is given by [28]

$$Y = F \cdot X, \quad \textbf{(11)}$$

where *Y* is the observed image, *F* is the speckle, and *X* is the true image. It is demonstrated that the log-cumulant of any order of *Y* is defined by the sum of the log-cumulant of the same order of *F* and *X* [31].

Particularly, the first two log-cumulants of *Y* can be specified by

$$\tilde{k}_{Y(1)} = \tilde{k}_{F(1)} + \tilde{k}_{X(1)}, \tilde{k}_{Y(2)} = \tilde{k}_{F(2)} + \tilde{k}_{X(2)}. \quad \textbf{(12)}$$

here, $\tilde{k}_{Y(1)}$ and $\tilde{k}_{Y(2)}$ can be assessed empirically from the image based on Eq. (10). Obviously, the parameters *M* and μ required for the Fisher MAP filter can be estimated from the image. Recalling the construction of the Fisher MAP filter, the speckle and the ground truth image are modeled by the Gamma and inverse Gamma distributions, respectively. Substituting (3) into (7), (8), and (9) successively, the first two log-cumulants of speckle are given by

$$\tilde{k}_{F(1)} = \psi(L) - \ln L, \tilde{k}_{F(2)} = \psi(1, L), \quad \textbf{(13)}$$

where $\psi(\cdot)$ denotes the Digamma function, and $\psi(1, L)$ denotes the Trigamma function [31].

Similarly, the first two log-cumulants of the true image is derived by

$$\tilde{k}_{X(1)} = \ln(\frac{M}{\mu}) - \psi(M), \tilde{k}_{X(2)} = \psi(1, M). \quad \textbf{(14)}$$

Substituting (13) and (14) into (12), *M* and μ can be estimated as:

$$\psi(1, \hat{M}) = \hat{\tilde{k}}_{Y(2)} - \psi(1, L), \quad \textbf{(15)}$$

$$\hat{\mu} = \frac{\hat{M}}{e^{\hat{\tilde{k}}_{Y(1)} + \psi(\hat{M}) - \psi(L) + \ln L}}. \quad \textbf{(16)}$$

here, $\hat{\tilde{k}}_{Y(1)}$ and $\hat{\tilde{k}}_{Y(2)}$ are the estimated values of the first two log-cumulants of *Y* respectively, which are calculated from the observe image by using Eq. (10).

As the Trigamma function $\psi(1,\cdot)$ is monotonous, the shape parameter *M* can be estimated from Eq. (15) by using bisection [34], and the scale parameter μ can be readily computed by Eq. (16).

5 Improved Fisher MAP Filter Based On Structural Information Detection

Based on structural information, the Fisher MAP filter is improved to yield better balance between speckle suppression and structural information (i.e., edges, fine details, and point targets) preservation [23]. The structure diagram of the improved Fisher MAP filter is provided in Figure 3.

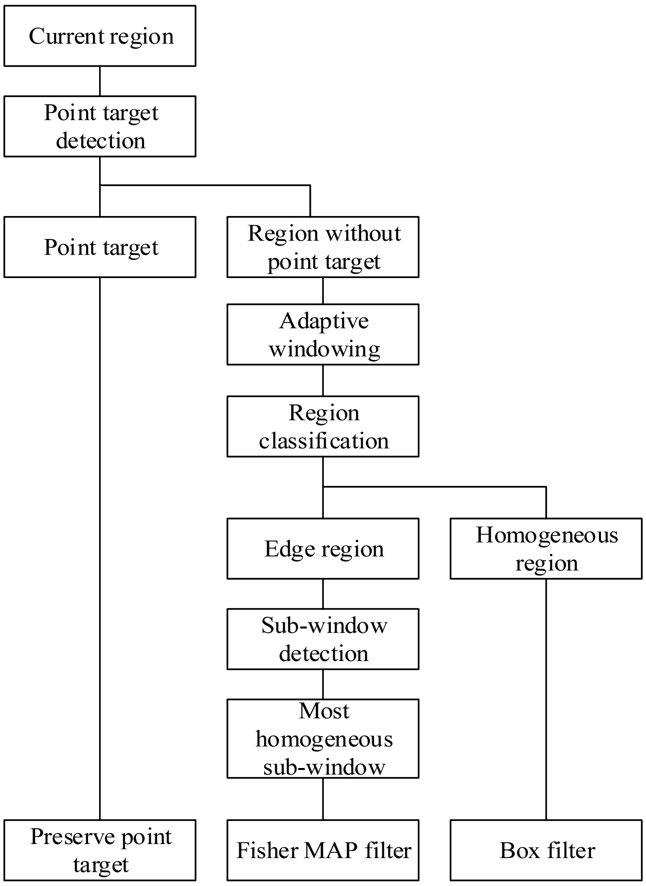

Figure 3. Structure chart of the improved Fisher MAP filter that uses structural information detection

The algorithm starts from the smallest 3 by 3 window for each pixel of image. Firstly, the point target is found by comparing the coefficient of variation (CoV) with the upper threshold. If the CoV is greater than the upper threshold, the point target appears, and its value is directly preserved. Next, the adaptive windowing is adopted to get the size of sliding window. The size of window is gradually adjusted by comparing the CoV of boundary pixels in a current window with the adaptive threshold. When the CoV is smaller than the threshold, the current window enlarges until it meets the predefined maximum window.

Finally, the sliding window to which the adaptive windowing method leads is classified by its heterogeneity. If sliding window belongs to heterogeneous regions where edges and fine details appear, sliding window is divided into eight directional sub-windows. By calculating the coefficient of variation for each sub-window, the most homogeneous sub-window with the lowest variation coefficient is chosen as the filtering region, which tends to efficiently suppress speckle in edge regions. Obviously, the improved Fisher MAP filter based on structural information detection can lead to better performance in comparison with the fixed-size Fisher MAP filter.

6 Despeckling Experiments

The improved Fisher MAP filter based on structural information detection was tested on two HR-SAR images. The SAR image and its despeckling results are shown in Figure 4. The classical Gamma MAP filter based on Gamma prior distribution was provided for comparison [26, 35]. The performance of various filters is evaluated in Table 1. *ENL* is the equivalent number of looks, and bigger values of *ENL* denote stronger speckle suppression [36-37]. *DCV* is defined by the difference of coefficient of variations between the filtered image and the true image in an edge region. Smaller values of *DCV* denote better edge preservation [38-67].

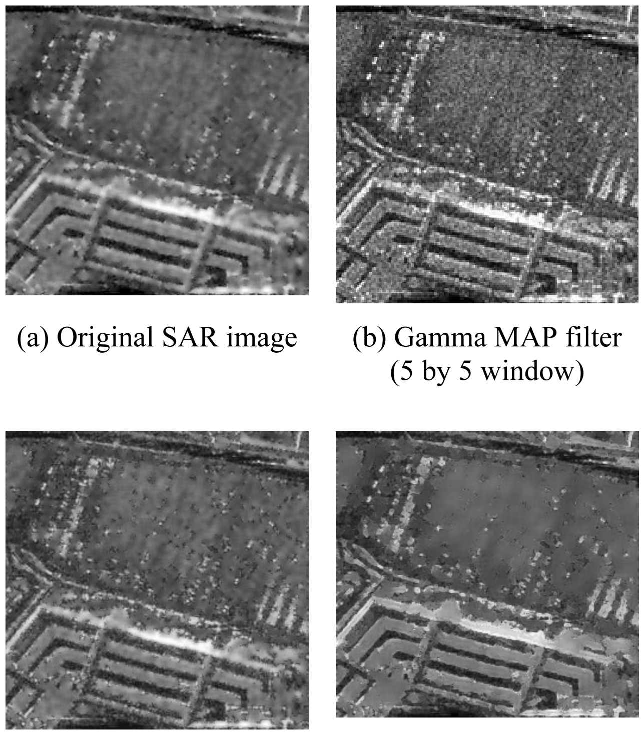

(a) Original SAR image

(b) Gamma MAP filter (5 by 5 window)

(c) Fisher MAP filter (5 by 5 window)

(d) Improved Fisher MAP filter (3 by 3 minimum window and 11 by 11 maximum window)

Figure 4. Despeckling results

Obviously, the Fisher MAP filter preserves edges, fine details, and point targets are much better when compared to the Gamma MAP filter, at the cost of some speckle that still exists in homogeneous regions and in edge regions. Integrating the effective preservation of edges, fine details, and point targets with the sufficient speckle suppression, the improved Fisher MAP filter based on structural information detection achieves the best performance that yields the biggest ENL and the smallest DCV .

The second SAR image and its despeckling results are given in Figure 5. The speckle pattern shown in Figure 6 is used to evaluate filter performance [27, 29]. Obviously, compared to the fixed-size Fisher MAP filter, the improved Fisher MAP filter based on structural information detection preserves edges and smoothes the speckle effectively.

(a) Original SAR image

(b) Fisher MAP filter (5 by 5 window)

(c) Improved Fisher MAP filter (3 by 3 minimum window and 11 by 11 maximum window)

Figure 5. Despeckling results

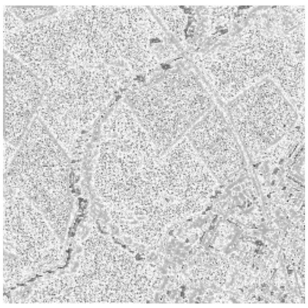

(a) Fisher MAP filter

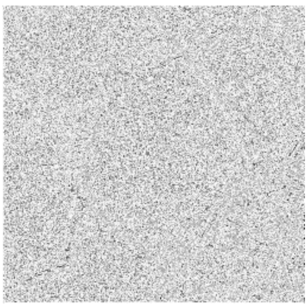

(b) Improved Fisher MAP filter

Figure 6. Speckle pattern corresponding to Figure 5

Table 1. Quantitative measures evaluating various filters in Figure 4

	ENL	DCV
Gamma MAP filter	96.2423	0.4635
Fisher MAP filter	52.9435	0.4547
improved Fisher MAP filter	122.9742	0.4491

7 Conclusion

Due to its high-peaked and heavy-tailed characteristics as well as its theoretical justification and mathematical tractability, the Fisher distribution is a popular choice for modeling HR-SAR images. Here, a Fisher MAP filter based on the Fisher model has been suggested. In this model, the parameter of image is regarded to be fixed to correspond to the formation mechanism of multi-look intensity images, and the other two parameters are accurately estimated from the image based on the second-kind statistics. In order to enhance the performance of the Fisher MAP filter especially in the aspect of speckle suppression, the Fisher MAP filter based on structural information detection has been proposed. The improved Fisher MAP filter, which successively performs the point target detection, the adaptive windowing, the homogeneous region detection, and the selection of the most homogeneous sub-window, leads to well-balanced performance between speckle suppression and edge detection. Despeckling experiments on HR-SAR images demonstrate that, compared to the fixed-size Fisher MAP filter, the proposed improved Fisher MAP filter based on structural information detection can preserve edges, fine details, and point targets more effectively, and is able to subdue speckle in homogeneous and edge regions much more sufficiently.

Acknowledgments

We are grateful to the Sandia National Laboratories for supplying us with high-resolution SAR images. This job is supported by the National key R&D Program of China under Grant NO. 2018YFB0203901. This work is supported by the National Natural Science Foundation of China (No. 61702091). This job is also supported by the Key Research and Development Program of Shaanxi Province (No.2018ZDXM-GY-036), the Shaanxi Key Laboratory of Intelligent Processing for Big Energy Data (No. IPBED7), the Fundamental Research Funds for the Central Universities (No. 2572018BH06, GK201903085), the Provincial Natural Science Foundation (No. F2015037), the Key Laboratory of Land Satellite Remote Sensing Application Center, Ministry of Natural Resources of the People's Republic of China (No. KLSMNR-202004) and the State Key Laboratory of Geo-Information Engineering (No. SKLGIE2019-M-3-5).

Declaration of Interest

The authors have no interest to declare.

References

[1] C. Oliver, S. Quegan, *Understanding Synthetic Aperture Radar Images*, Boston, MA: Artech House, 1998.

[2] H. Choi, J. Jeong, Speckle noise reduction technique for sar images using statistical characteristics of speckle noise and discrete wavelet transform, *Remote Sensing*, Vol. 11, No. 10, Article No. 1184, May, 2019. DOI: 10.3390/rs11101184.

[3] R. Jin, F. Gini, M. Greco, J. Yin, J. Yang, Statistical modeling of SAR images with the generalized beta distribution of the first kind, *International Conference on Radar Systems (Radar 2017)*, Belfast, UK, 2017, pp. 1-5.

[4] H. Sportouche, J. Nicolas, F. Tupin, Mimic capacity of fisher and generalized gamma distributions for high-resolution SAR image statistical modeling, *IEEE Journal of Selected Topics in Applied Earth Observations and Remote Sensing*, Vol. 10, No. 12, pp. 5695-5711, December, 2017. DOI: 10.1109/JSTARS.2017.2747118.

[5] K. Wang, X. Yu, S. Gou, Classification of heterogeneous scenes in POL-SAR image based on statistical analysis, *IEEE Region 10 Annual International Conference, Proceedings/TENCON*, Jeju, South Korea, 2018, pp. 2164-2169. DOI: 10.1109/TENCON.2018.8650079.

[6] C. Wang, W. Su, H. Gu, H. Shao, SAR image modeling based on the mixture gamma heavy-tailed rayleigh distribution, *Cehui Xuebao/Acta Geodaetica Et Cartographica Sinica*, Vol. 43, No. 2, pp. 151-157, February, 2014. DOI: 10.13485/j.cnki.11-2089.2014.0022.

[7] C. Tison, J. M. Nicolas, F. Tupin, H. Maitre, A new statistical model for Markovian classification of urban areas in high-resolution SAR images, *IEEE Transactions on Geoscience and Remote Sensing*, Vol. 42, No. 10, pp. 2046-2057, October, 2004.

[8] E. E. Kuruoglu, J. Zerubia, Modeling SAR images with a generalization of the Rayleigh distribution, *IEEE Transactions on Image Processing*, Vol. 13, No. 4, pp. 527-533, April, 2004.

[9] Y. Peng, J. Chen, X. Xu, F. Pu, SAR images statistical modeling and classification based on the mixture of alpha-stable distributions, *Remote Sensing*, Vol. 5, No. 5, pp. 2145-2163, May, 2013.

[10] M. S. Greco, F. Gini, Statistical analysis of high-resolution SAR ground clutter data, *IEEE Transactions on Geoscience and Remote Sensing*, Vol. 45, No. 3, pp. 566-575, March, 2007.

[11] H. Rinne, *The Weibull Distribution: A Handbook*, Boca Raton: CRC Press, 2009.

[12] A. Karine, A. Toumi, A. Khenchaf, M. El Hassouni, Target recognition in radar images using weighted statistical dictionary-based sparse representation, *IEEE Geoscience and Remote Sensing Letters*, Vol. 14, No. 12, pp. 2403-2407, December, 2017. DOI: 10.1109/LGRS.2017.2766225.

[13] D. K. Mahapatra, K. R. Pradhan, L. P. Roy, An experiment on MSTAR data for CFAR detection in lognormal and weibull distributed sar clutter, *2015 International Conference on Microwave, Optical and Communication Engineering, ICMOCE 2015*, Bhubaneswar, India, 2015, pp. 377-380. DOI: 10.1109/ICMOCE.2015.7489771.

[14] J. Sun, X. Wang, X. Yuan, Q. Zhang, C. Guan, A. V. Babanin, The dependence of sea SAR image distribution parameters on surface wave characteristics, *Remote Sensing*, Vol. 10, No. 11, Article No. 1843, November, 2018. DOI: 10.3390/rs10111843.

[15] D. Guan, D. Xiang, X. Tang, G. Kuang, SAR image despeckling based on nonlocal low-rank regularization, *IEEE Transactions on Geoscience and Remote Sensing*, Vol. 57, No. 6, pp. 3472-3489, June, 2019. DOI: 10.1109/TGRS.2018.2885089.

[16] C. Liu, H.-C. Li, X. Sun, W. J. Emery, H distribution for multilook polarimetric SAR data, *IEEE Geoscience and Remote Sensing Letters*, Vol. 14, No. 4, pp. 489-493, April, 2017. DOI: 10.1109/LGRS.2017.2650898.

[17] H. Sportouche, J.-M. Nicolas, F. Tupin, Mimic capacity of fisher and generalized gamma distributions for high-resolution SAR image statistical modeling, *IEEE Journal of Selected Topics in Applied Earth Observations and Remote Sensing*, Vol. 10, No. 12, pp. 5695-5711, December, 2017. DOI: 10.1109/JSTARS.2017.2747118.

[18] H. Li, W. Hong, Y. Wu, P. Fan, An efficient and flexible statistical model based on generalized Gamma distribution for amplitude SAR images, *IEEE Transactions on Geoscience and Remote Sensing*, Vol. 48, No. 6, pp. 2711-2722, June, 2010.

[19] H. Li, W. Hong, Y. Wu, P. Fan, Bayesian wavelet shrinkage with heterogeneity-adaptive threshold for SAR image despeckling based on generalized Gamma distribution, *IEEE Transactions on Geoscience and Remote Sensing*, Vol. 51, No. 4, pp. 2388-2402, April, 2013.

[20] H. Li, W. Hong, Y. Wu, P. Fan, On the empirical-statistical modeling of SAR images with generalized Gamma distribution, *IEEE Journal of Selected Topics in Signal Processing*, Vol. 5, No. 3, pp. 386-397, June, 2011.

[21] S. Cui, M. Datcu, Statistical wavelet subband modeling for multi-temporal SAR change detection, *IEEE Journal of Selected Topics in Applied Earth Observations and Remote Sensing*, Vol. 5, No. 4, pp. 1095-1109, August, 2012.

[22] Z. Sun, C. Han, Modeling high-resolution synthetic aperture radar images with heavy-tailed distributions, *Acta Physica Sinica*, Vol. 59, No. 2, pp. 998-1008, February, 2010.

[23] Z. Sun, C. Han, Combined despeckling algorithm of synthetic aperture radar images based on region classification, adaptive windowing and structure detection, *Acta Physica Sinica*, Vol. 59, No. 5, pp. 3210-3220, May, 2010.

[24] F. Liu, P. Chen, Y. Li, L. Jiao, D. Cui, Y. Cui, J. Gu, Structural feature learning-based unsupervised semantic segmentation of synthetic aperture radar image, *Journal of Applied Remote Sensing*, Vol. 13, No. 1, Article No. 014501, January, 2019. DOI: 10.1117/1.JRS.13.014501.

[25] Z. Liu, G. Li, G. Mercier, Y. He, and Q. Pan, Change

detection in heterogenous remote sensing images via homogeneous pixel transformation, *IEEE Transactions on Image Processing*, Vol. 27, No. 4, pp. 1822-1834, April, 2018. DOI: 10.1109/TIP.2017.2784560.

[26] S. Solbo and T. Eltoft, Γ-WMAP: a statistical speckle filter operating in the wavelet domain, *International Journal of Remote Sensing*, Vol. 25, No. 5, pp. 1019-1036, March, 2004.

[27] Z. Sun, D. Lin, W. Wei, M. Woźniak and R. Damaševičius, Road Detection Based on Shearlet for GF-3 Synthetic Aperture Radar Images, *IEEE Access*, Vol. 8, pp. 28133-28141, January, 2020. DOI: 10.1109/ACCESS.2020.2966580.

[28] B. Zhou, X. Duan, D. Ye, W. Wei, M. Woźniak, D. Połap, and R. Damaševičius, Multi-level features extraction for discontinuous target tracking in remote sensing image monitoring, *Sensors*, Vol. 19, No. 22, Article No. 4855, November, 2019. DOI: 10.3390/s19224855.

[29] Z. Sun and C. Han, Maximum a posteriori filtering for synthetic aperture radar images based on heavy-tailed Rayleigh distribution of speckle, *Acta Physica Sinica*, Vol. 56, No. 8, pp. 4565-4570, August, 2007.

[30] Z. Sun, Gamma-distributed maximum a posteriori despeckling algorithm of high-resolution synthetic aperture radar images, *Acta Physica Sinica*, Vol. 62, No. 18, pp. 1-6, September, 2013.

[31] Z. Sun, Parameter estimation of inverse Gamma distribution of RCS for SAR images based on second-kind statistics, *Proceedings of the 18th China Symposium on Remote Sensing*, Wuhan, China, 2012, pp. 298-302.

[32] S. Cui, G. Schwarz, and M. Datcu, A comparative study of statistical models for multilook SAR images, *IEEE Geoscience and Remote Sensing Letters*, Vol. 11, No. 10, pp. 1752-1756, October, 2014.

[33] A. Achim, E. E. Kuruoğlu, J. Zerubia, SAR image filtering based on the heavy-tailed rayleigh model, *IEEE Transactions on Image Processing*, Vol. 15, No. 9, pp. 2686-2693, September, 2006. DOI: 10.1109/TIP.2006.877362.

[34] S. Chen, J. Liu, G. Wang, Q. Li, SAR image adaptive MAP filtering based on the generalized Gaussian model, *Proceedings of SPIE - MIPPR 2007: Multispectral Image Processing*, Vol. 6787, Article No. 678711, November, 2007. DOI: 10.1117/12.749035.

[35] A. Baraldi, F. Parmiggiani, A refined Gamma MAP SAR speckle filter with improved geometrical adaptivity, *IEEE Transactions on Geoscience and Remote Sensing*, Vol. 33, No. 5, pp. 1245-1257, September, 1995.

[36] A. Lapini, T. Bianchi, F. Argenti, L. Alparone, Blind speckle decorrelation for SAR image despeckling, *IEEE Transactions on Geoscience and Remote Sensing*, Vol. 52, No. 2, pp. 1044-1058, February, 2014.

[37] J. J. Ranjani, S. J. Thiruvengadam, Generalized SAR despeckling based on DTCWT exploiting interscale and intrascale dependences, *IEEE Geoscience and Remote Sensing Letters*, Vol. 8, No. 3, pp. 552-556, May, 2011.

[38] W. Wei, Y. Qi, Information potential fields navigation in wireless Ad-Hoc sensor networks, *Sensors*, Vol. 11, No. 5, pp. 4794-4807, May, 2011.

[39] W. Wei, X. Fan, H. Song, X. Fan, J. Yang, Imperfect information dynamic stackelberg game based resource allocation using hidden markov for cloud computing, *IEEE Transactions on Services Computing*, Vol. 11, No. 1, pp. 78-89, January-February, 2018. DOI: 10.1109/TSC.2016.2528246.

[40] W. Wei, H. Song, W. Li, P. Shen, A. Vasilakos, Gradient-driven parking navigation using a continuous information potential field based on wireless sensor network, *Information Sciences*, Vol. 408, pp. 100-114, October, 2017. DOI: 10. 1016/j.ins.2017.04.042.

[41] W. Wei, Q. Xu, L. Wang, X. H. Hei, P. Shen, W. Shi, L. Shan, GI/Geom/1 queue based on communication model for mesh networks, *International Journal of Communication Systems*, Vol. 27, No. 11, pp. 3013-3029, November, 2014.

[42] W. Wei, Z. Sun, H. Song, H. Wang, X. Fan, X. Chen, Energy Balance-Based Steerable Arguments Coverage Method in WSNs, *IEEE Access*, Vol. 6, pp. 33766-33773, March, 2017. DOI: 10.1109/ACCESS.2017.2682845.

[43] W. Wei, H. Song, H. Wang, X. Fan, Research and Simulation of Queue Management Algorithms in Ad Hoc Networks under DDoS Attack, *IEEE Access*, Vol. 5, pp. 27810-27817, March, 2017. DOI: 10.1109/ACCESS.2017. 2681684.

[44] W. Wei, X. Fan, H. Song, H. Wang, Video tamper detection based on multi-scale mutual information, *Multimedia Tools and Applications*, Vol. 78, No. 19, pp. 27109-27126, October, 2019. DOI: 10.1007/s11042-017-5083-1.

[45] W. Wei, X.-L. Yang, B. Zhou, J. Feng, P.-Y. Shen, Combined energy minimization for image reconstruction from few views, *Mathematical Problems in Engineering*, Vol. 2012, Article ID 154630, October, 2012.

[46] W. Wei, X.-L. Yang, P.-Y. Shen, B. Zhou, Holes detection in anisotropic sensornets: Topological methods, *International Journal of Distributed Sensor Networks*, Vol. 8, No. 10, Article ID 135054, October, 2012.

[47] W. Wei, Y. Qiang, J. Zhang, A Bijection between Lattice-Valued Filters and Lattice-Valued Congruences in Residuated Lattices, *Mathematical Problems in Engineering*, Vol. 2013, Article ID 908623, July, 2013.

[48] W. Wei, H. M. Srivastava, Y. Zhang, L. Wang, P. Shen, J. Zhang, A local fractional integral inequality on fractal space analogous to Anderson's inequality, *Abstract and Applied Analysis*, Vol. 2014, Article ID 797561, June, 2014.

[49] W. Wei, S. Liu, W. Li, D. Du, Fractal Intelligent Privacy Protection in Online Social Network Using Attribute-Based Encryption Schemes, *IEEE Transactions on Computational Social Systems*, Vol. 5, No. 3, pp. 736-747, September, 2018.

[50] W. Wei, X. Fan, M. Woźniak, H. Song, W. Li, Y. Li, P. Shen, H∞ Control of Network Control System for Singular Plant, *Information Technology And Control*, Vol. 47, No. 1, pp. 140-150, March, 2018.

[51] Q. Ke, J. Zhang, H. Song, Y. Wan, Big Data Analytics Enabled by Feature Extraction Based on Partial Independence, *Neurocomputing*, Vol. 288, pp. 3-10, May, 2018. DOI: 10.1016/j.neucom.2017.07.072.

[52] Q. Ke, J. Zhang, W. Wei, D. Połap, M. Woźniak, L. Kośmider, R. Damaševĭcius, A neuro-heuristic approach for

recognition of lung diseases from X-ray images, *Expert Systems with Applications*, Vol. 126, pp. 218-232, July, 2019. https://doi.org/10.1016/j.eswa.2019.01.060.

[53] Q. Ke, J. Zhang, W. Wei, R. Damasevicius, M. Wozniak, Adaptive Independent Subspace Analysis of Brain Magnetic Resonance Imaging Data, *IEEE Access*, Vol. 7, pp. 12252-12261, January, 2019. DOI: 10.1109/ACCESS.2019.2893496.

[54] Q. Ke, J. Zhang, M. Wozniak, W. Wei, The Phase and Shift-invariant Feature by Adaptive Independent Subspace Analysis for Cortical Complex Cells, *Information technology and control*, Vol. 48, No. 1, pp. 58-70, March, 2019.

[55] W. Wei, J. Su, H. Song, H. Wang, X. Fan, Cdma-based anti-collision algorithm for epc global c1 gen2 systems, *Telecommunication Systems*, Vol. 67, No. 1, pp. 63-71, January, 2018.

[56] S. Xia, Y. Liu, X. Ding, X. Wang, H. Yu, Y. Luo, Granular ball computing classifiers for efficient, scala-ble and robust learning, *Information Sciences*, Vol. 483, pp. 136-152, May, 2019.

[57] S. Xia, D. Peng, D. Meng, C. Zhang, G. Wang, E. Giem, W. Wei, Z. Chen, A Fast Adaptive k-means with No Bounds, *IEEE Transactions on Pattern Analysis and Machine Intelligence*, July, 2020, pp. 1-1 DOI: 10.1109/TPAMI.2020.3008694.

[58] J. Su, Z. Sheng, L. Xie, G. Li, A. X. Liu, Fast splitting-based tag identification algorithm for anti-collision in UHF RFID system, *IEEE Transactions on Communications*, Vol. 67, No. 3, pp. 2527-2538, March, 2019. DOI: 10.1109/TCOMM.2018.2884001.

[59] J. Su, Z. Sheng, V. C. M. Leung, Y. Chen, Energy efficient tag identification algorithms for RFID: survey, motivation and new design, *IEEE Wireless Communications*, Vol. 26, No. 3, pp. 118-124, June, 2019.

[60] S. Xia, Y. Liu, X. Ding, G. Wang, H. Yu, Y. Luo, Granular ball computing classifiers for efficient, scalable and robust learning, *Information Sciences*, Vol. 483, pp. 136-152, May, 2019.

[61] S. Qi, Y. Zheng, X. Chen, W. Wei, Ants can Carry Cheese: Secure and Private RFID-Enabled Third-Party Distribution, *IEEE Transactions on Dependable and Secure Computing*, pp. 1-1, September, 2020. DOI: 10.1109/TDSC. 2020.3026191.

[62] S. Qi, Y. Lu, W. Wei, X. Chen, Efficient Data Access Control with Fine-Grained Data Protection in Cloud-Assisted IIoT, *IEEE Internet of Things Journal*, Vol. 8, No. 4, pp. 2886-2899, February, 2021. DOI: 10.1109/JIOT.2020.3020979.

[63] Q. Ke, J. Zhang, H. Song, Y. Wan, Big data analytics enabled by feature extraction based on partial independence, *Neurocomputing*, Vol. 288, pp.3-10, May, 2018.

[64] M. Liu, W. Wei, B. Xu, H. Wang, Study on Dynamic Multi-document Summarization System Framework Method, *Journal of Internet Technology*, Vol. 19, No. 5, pp. 1339-1346, September, 2018.

[65] L. K. Ramasamy, S. Kadry, M. A. Jayanthi, W. Wei, S. Rho, Handling Failures in Semantic Web Service Composition Through Replacement Policy in Healthcare Domain, *Journal of Internet Technology*, Vol. 21, No. 3, pp. 733-741, May, 2020.

[66] M. Zhou, Z. Bai, T. Yi, X. Chen, W. Wei, Performance Predict Method Based on Neural Architecture Search, *Journal of Internet Technology*, Vol. 21, No. 2, pp. 385-392, March, 2020.

[67] X. Sun, Y. Liu, W. Wei, W. Jing, C. Zhao, Based on QoS and Energy Efficiency Virtual Machines Consolidation Techniques in Cloud, *Journal of Internet Technology*, Vol. 20, No. 6. pp. 1849-1859, November, 2019.

Biographies

Wei Wei (SM'17) received the M.S. and Ph.D. degrees from Xi'an Jiaotong University, Xi'an, China, in 2005 and 2011, respectively. He is currently an Associate Professor with the School of Computer Science and Engineering, Xi'an University of Technology, Xi'an. He ran many funded research projects as principal investigator and technical members. His current research interests include the area of wireless networks, wireless sensor networks application, image processing, mobile computing, distributed computing, and pervasive computing, Internet of Things, and sensor data clouds. He has published around 100 research papers in international conferences and journals. Dr. Wei is a Senior Member of the China Computer Federation. He is an Editorial Board Member of the Future Generation Computer System, the IEEE Access, Ad Hoc & Sensor Wireless Sensor Network, The Institute of Electronics, Information and Communication Engineers, and KSII Transactions on Internet and Information Systems. He is a TPC member of many conferences and a regular Reviewer of the IEEE Transactions on Parallel and Distributed Systems, the IEEE Transactions on Image Processing, the IEEE Transactions on Mobile Computing, the IEEE Transactions on Wireless Communications, the Journal of Network and Computer Applications, and many other Elsevier journals. the causes and solutions of congestion, and devoted herself to studying the division mode of the traffic control sub-area.

Zeng-Guo Sun was born in Xi'an, Shaanxi, China, in 1980. He received his bachelor's degree in Computer Science and Technology in 2003, and PhD degree in Control Science and Engineering in 2010, all from the Xi'an Jiaotong University. He was a visiting scholar in Pennsylvania State University from 2007 to 2008. Now he is an Associate Professor in Shaanxi Normal University. His research interests are in radar image processing.

Zhi-Hua Zhang was born in Zhumadian, Henan, China, in 1988. He received his bachelor's degree in Communication Engineering from Nanyang Normal University, in 2012. He received his master's degree in Pattern Recognition and Intelligent System from Huaqiao University, in 2015. His research interests are in radar image processing.

Rafał Scherer received his MSc degree in computer science from the Czestochowa University of Technology, Poland, in 1997 and his PhD in 2002 from the same university. Currently, he is an associate professor at Czestochowa University of Technology. His present research interests include machine learning and neural networks for image processing, computer system security, prediction and classification.

Robertas Damaševičius CIUS graduated at the Faculty of Informatics, Kaunas University of Technology (KTU) in Kaunas, Lithuania in 1999, where he received a B.Sc. degree in Informatics. He finished his M.Sc. studies in 2001 (cum laude), and he defended his Ph.D. thesis at the same University in 2005. Currently, he is a Professor at Software Engineering Department, KTU and lectures robot programming and software maintenance courses. His research interests include brain-computer interface, bioinformatics, data mining and machine learning. He is the author or co-author of over 100 papers as well as a monograph published by Springer.